C. R. Mecanique 339 (2011) 458–465

Contents lists available at ScienceDirect

Comptes Rendus Mecanique

www.sciencedirect.com

Surface mechanics: facts and numerical models

Extending the contact regimes to single-crystal indentations

Jorge Alcalá *, Daniel Esqué-de los Ojos

GRICCA-EUETIB, Universitat Politècnica de Catalunya, Comte d'Urgell 187, 08036 Barcelona, Spain

ARTICLE INFO

Article history:
Available online 21 June 2011

Keywords:
Indentation and hardness
Plasticity
Contact mechanics
Finite elements

ABSTRACT

This article provides a fresh look into the concept of the contact regimes in mechanistic analyses of indentation experiments performed in single crystals. In this context, spherical microindentation experiments in fcc metals are examined through detailed continuum crystal plasticity finite element simulations in order to provide meaning to the onset of fully-plastic and elasto-plastic contact regimes, which are well-known to rule the behavior of polycrystals exhibiting isotropic uniaxial stress–strain curves. Attention is then given to evaluate the applicability of Tabor's hardness relation in ruling fully-plastic single-crystal spherical indentations as well as the extraction of the uniaxial plastic flow properties from a series of microindentation tests performed at different penetrations. A discussion is finally provided on the applicability of self-similarity assumptions to the analysis of single-crystal fully-plastic indentations.

1. Introduction

Indentation experiments are extensively used to probe the mechanical properties of surfaces. A distinctive feature to these experiments is their flexibility in assessing the mechanical response from small microscopic length scales, where dislocation nucleation phenomena occur during pop-in excursions in load–penetration depth curves, to large macroscopic scales where the imprint encompasses a number of grains. In the latter macroscopic length scales, the widely accepted framework to the interpretation of the experiments is rooted in slip-line field derivations for perfectly-plastic solids and self-similarity analyses (see, e.g., [1–4]). This has led to the conception of the contact regimes, where hardness evolves from that for a perfectly-elastic behavior to an elasto-plastic regime to a fully-plastic indentation response. The spherical indentation behavior is paradigmatic to such transition as full-plasticity is gradually favored with increasing penetration of the tip into the surface.

Elasto-plastic indentations are usually analyzed within the framework of cavity expansion problems, where material sinking-in effects are assumed to occur at the contact boundary (see, e.g., [5–9]). The analysis of the experiments follows the early work by Hill and by Johnson [1] for perfectly-plastic solids which has then been extended to strain hardening media. Fully-plastic indentation finally dominates with increasing penetration thus following Tabor's hardness empirical formula [4,10]

$$\bar{p} = 2.8\sigma_{\circ}\left(0.4\frac{a}{D}\right)^{n} \tag{1}$$

where $\bar{p}$ is the hardness measured at a particular ratio of the imprint radius to indenter's tip diameter, a/D, in materials whose plastic uniaxial stress (σ)–strain (ϵ) relation follows a power-law hardening model with flow stress $\sigma_{\circ}$:

* Corresponding author.
E-mail address: jorge.alcala@upc.edu (J. Alcalá).

1631-0721/$ – see front matter
doi:10.1016/j.crme.2011.05.004

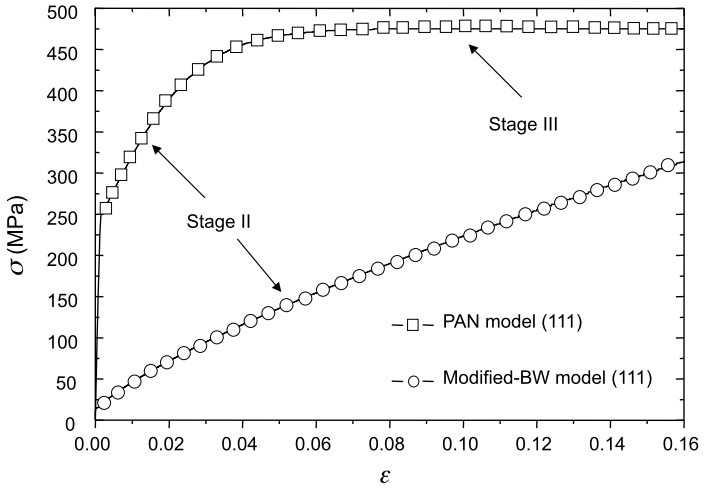

Fig. 1. Uniaxial stress–strain curves for pure copper (modified-BW model) and Al–Cu (PAN model) along a highly symmetric (111) orientation favoring multiple glide (cross-hardening) conditions. The figure shows development of multiple glide deformation stage-II and the strong saturation of strain hardening occurring in the PAN model during deformation stage-III.

$$\sigma = \sigma_\circ \epsilon^n \tag{2}$$

By invoking continuity between the elastic and plastic branches of the σ–ϵ curve, it then follows that

$$\sigma_{ys} = \sigma_\circ \epsilon_{ys}^n; \qquad \epsilon_{ys} = \sigma_{ys}/E \tag{3}$$

where subscript ys denotes the onset of plastic yielding and E is the Young's modulus. Hence,

$$\sigma_\circ = E^n {\sigma_{ys}}^{1-n} \tag{4}$$

A mechanistic basis to Eq. (1) was first given by Hill et al. [10] under the assumption of self-similar indentation behaviors where: (i) the plastic zone size scales in proportion with contact radius a in the same manner as the amount of material pile-up or sinking-in at the contact boundary is assumed to be an invariant of the indentation process; (ii) the condition of *plastic*-similarity is enforced through a rigid power-law function such as in Eq. (2), where linear elasticity is neglected (i.e., a non-vanishing value of flow stress $\sigma_\circ$ is imposed in Eq. (2) by disregarding Eq. (4) for the specific condition of $\sigma_{ys} = 0$); and (iii) small penetrations are enforced so that the spherical tip can be substituted by a best-fit parabolic, and thus *geometrically*-similar, indenter shape. In self-similar indentation analyses, a constant value for parameter c^2 is therefore taken, measuring the relative amount of pile-up/sinking-in as [10]

$$c^2 \equiv h/h_s \approx a^2/h_s D \tag{5}$$

where h is the penetration depth marking the height of the contact boundary and h_s is the penetration measured from the original (undeformed) surface.

An important normalizing parameter introduced by Johnson that measures transition from elasto-plastic to fully-plastic indentation behaviors is $aE/D\sigma_\circ$ [1]. This stems from the argument that the severity of the deformation state underneath the indenter increases with a/D while, concurrently, the resulting response becomes increasingly plastic for solids with a large E and a small flow stress $\sigma_\circ$. Hence, large values of $aE/D\sigma_\circ$ mark attainment of the fully-plastic indentation regime while elasto-plasticity prevails as this factor decreases towards the elastic (Hertzian) prediction of $aE/D\sigma_\circ \approx 1.1$ [1].

Although the above investigations by Tabor, Hill and Johnson set the basis to the extraction of mechanical properties from spherical indentation experiments, this topic continues to receive intensive research efforts through measurements of both hardness evolutions and applied load–penetration depth curves (see, e.g., [11–19]).

The purpose of this work is to check the applicability of the above framework in the analysis of indentation experiments performed at mesoscopic length scales where the imprint is fully embedded within a single grain or microstructural unit of material. We thus seek to apply continuum crystal plasticity analyses to indentation experiments [20–26] with the aim of evaluating: (i) the validity of Tabor's relation in describing fully-plastic indentations; (ii) the underlying plastic flow features in the evolution from elasto-plasticity to full-plasticity; and (iii) the presumption of self-similar indentation responses in the scaling of both pile-up/sinking-in effects and the plastic zone size in fully-plastic indentations. With this in mind, we shall employ two crystal plasticity hardening models with the purpose of describing both weak and strong strain hardening crystals (Fig. 1). As discussed next, these descriptions provide some representation to the perfectly-plastic ($n \to 0$ with non-vanishing σ_{ys}) and plastically-similar power-law hardening ($n > 0$ with vanishing σ_{ys}) material models, which are respectively the focus to the above slip-line field and plastic-similarity analyses.

2. Finite element simulations

The present continuum crystal plasticity finite element simulations concern pure and alloyed fcc crystals. A key feature in the analysis involves hardening matrix $h_{\alpha\beta}$, dictating the increase in the critical resolved shear strength for dislocation gliding $\tau_\circ$ as in [27]

$$\dot{\tau}_\circ^{(\alpha)} = \sum_\beta h_{\alpha\beta}\,\dot{\gamma}^{(\beta)} \tag{6}$$

where superscript α denotes the primary slip system and β denotes the secondary slip system. Activation of secondary slip thus implies a non-vanishing term for the shear strain $\gamma^{(\beta)}$. Multiplication of the shear strain with the relevant component of matrix $h_{\alpha\beta}$ for the specific combination of slip systems α, β results in an increase in $\tau_\circ$.

The crystals under investigation undergo distinctly different hardening responses when subjected to uniaxial strains as prescribed by different formulations for matrix $h_{\alpha\beta}$. In particular, pure copper is modeled through the modified Bassani and Wu (BW) model described in detail in our previous work [24]. That is,

$$h_{\alpha\alpha} = \left\{(h_\circ - h_\mathrm{I})\,\mathrm{sech}^2\left[\frac{(h_\circ - h_\mathrm{I})\gamma^{(\alpha)}}{(\tau_\mathrm{s} - \tau_\circ)}\right] + h_\mathrm{I}\right\}\left\{1 + \sum_{\beta\neq\alpha} f_{\alpha\beta}\tanh\left(\frac{\gamma^{(\beta)}}{\gamma_\circ}\right)\right\}; \qquad h_{\alpha\beta} = 0 \tag{7}$$

where parameters $h_\circ$, h_I, τ_s and $\tau_\circ$ are fitted to reproduce the single-glide response of copper and $\gamma_\circ$ is fitted to capture its multiple glide (cross-hardening) behavior. The following summarizes the main features of this model. First, upon saturation of the argument in the hyperbolic secant with increasing shear strain in the primary slip system ($\gamma^{(\alpha)}$), the first term in curly brackets decays into parameter h_I that dictates strain hardening as a result of dislocation pile-up mechanisms in deformation stage-I. Secondary slip (cross-hardening) then activates as $\gamma^{(\beta)}$ increases from zero to the point where the hyperbolic tangent saturates at 1. Finally, matrix $f_{\alpha\beta}$ measures the relative strength of the different dislocation junctions in all slip systems during such deformation stage-II.

Following [24], it is found that, by virtue of Eqs. (A8) and (A11) [28]:

$$h_\mathrm{I} = \frac{\mu}{2K}\left[\kappa_{\alpha\alpha}\ln\left(b\sqrt{\rho^{(\alpha)}}\right)\right]^2 = 0.12\left[\ln\left(b\sqrt{\rho^{(\alpha)}}\right)\right]^2 \tag{8}$$

where $\rho^{(\alpha)}$ is the dislocation density in slip system α, b is the Burger's vector, μ is the shear modulus and K is a material parameter. It then naturally emerges that

$$f_{\alpha\beta} = \left(\frac{\kappa_{\alpha\beta}\ln(b\sqrt{\rho^{(\beta)}})}{\kappa_{\alpha\alpha}\ln(b\sqrt{\rho^{(\alpha)}})}\right)^2 \tag{9}$$

where $\kappa_{\alpha\beta}$ is a new physically-based matrix governing dislocation interactions according to molecular dynamics simulations for the different types of dislocation junctions. All parameters in the model are given in [24,28].

Alloyed Al–Cu crystals were modeled following the Peirce, Asaro and Needleman (PAN) hardening formulation [29,30]. The general features in the PAN model are the rapid development of cross-hardening deformation stage-II without any significant single-glide deformation stage-I, as well as a negligible hardening rate under saturation stage-III. Overall, these features are captured through [29,30]

$$h_{\alpha\alpha} = h(\gamma) = h_\circ\,\mathrm{sech}^2\left|\frac{h_\circ\gamma}{\tau_\mathrm{s} - \tau_\circ}\right|; \qquad h_{\alpha\beta} = q h_{\alpha\alpha} \tag{10}$$

where γ is the total (accumulative) shear strain in all slip systems:

$$\gamma = \sum_\alpha \int |\dot{\gamma}^{(\alpha)}|\,\mathrm{d}t \tag{11}$$

The above parameters $h_\circ$, τ_s and $\tau_\circ$ are also given in [24], where cross-hardening parameter $q = 1.2$ has been advocated in the present work. A fundamental difference between the two models emerges since the critical shear stress for dislocation gliding $\tau_\circ$ approaches 1 MPa in the modified-BW model while it increases to 60 MPa in the PAN formulation in order to account for the influence of alloying. Furthermore, the decay in hardening rate during deformation stage-III is more significant in the PAN than in the modified-BW models. These two features are illustrated in the stress–strain curves of Fig. 1.

Single-crystal indentations were simulated in the (111), (011) and (001) planes, where only the last are given here for simplicity. Nearly identical results are found for the remaining (111) and (011) planes as the degree of hardness anisotropy is smaller than 5% throughout the entire penetration range. In addition to the crystal plasticity simulations, complementary analyses were herein performed with the J_2-flow theory of plasticity with isotropic power-law hardening as described through Eqs. (2)–(4). This model is taken to reproduce the behavior of polycrystalline aggregates when subjected to indentation experiments [31]. Different values of $\sigma_\circ$, E and n were employed in such simulations with the purpose of reproducing

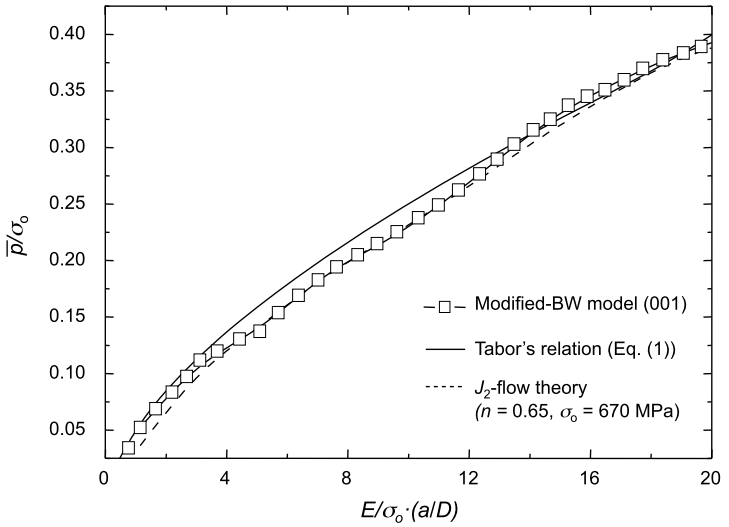

Fig. 2. Evolution of normalized hardness in pure copper deforming through the modified-BW model. The evolution predicted through Tabor's formula with inferred parameters $\sigma_\circ$ and n (see Table 1 and Eq. (12)) is superimposed along with the equivalent J_2-flow theory finite element simulation. Excellent accord is found for the three analyses in the entire penetration range.

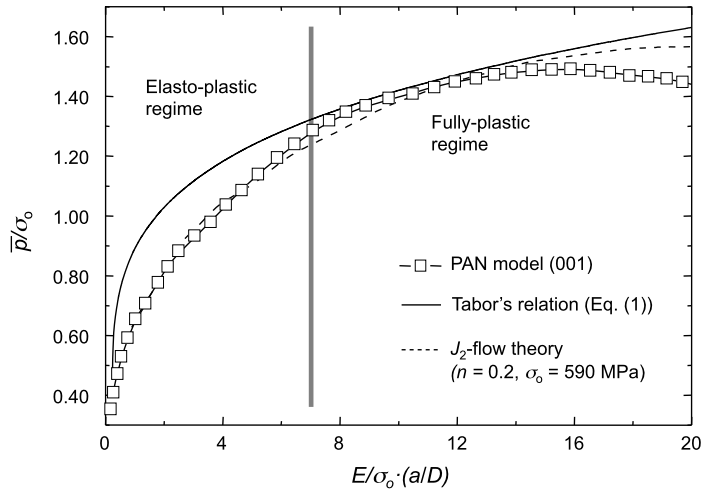

Fig. 3. Evolution of normalized hardness in Al–Cu crystals deforming through the PAN model. The evolution predicted through Tabor's formula with inferred parameters $\sigma_\circ$ and n is superimposed along with the equivalent J_2-flow theory finite element simulation (Table 1). Accordance is reached passed the critical penetration marking the fully-plastic indentation regime ($E/\sigma_\circ \cdot (a/D) > 7$) which is used to find parameters $\sigma_\circ$ and n through Eq. (12). Also, notice the hardness decay occurring at large penetrations in agreement with the onset of the perfect-plasticity dominated indentation regime described in [29] for polycrystalline aggregates deforming through the J_2-flow plasticity theory. See text for details.

the contact variables from the crystal plasticity simulations as described in Section 3. The same finite element meshes were used in both types of analyses to facilitate direct comparison of the results. Large strains and rotations were accounted for in all simulations.

3. The contact regimes and mechanical property extractions

An important aspect in indentation experiments performed with small indenter diameter D and contact radius a is the possible increase in hardness as compared to that measured with greater loads at identical a/D. This size-dependent response is connected with dislocation nucleation phenomena occurring at small applied loads that are not amenable to analysis through the present continuum mechanics scheme. In this context, it is important to clarify that the present investigation seeks to provide a fundamental clear-cut view into the onset of the contact regimes in single-crystal indentations at sufficiently large loads where the development of such size-dependent indentation responses can be neglected.

The evolutions of the normalized hardness $\bar{p}/\sigma_\circ$ with increasing parameter $aE/D\sigma_\circ$ for copper (modified-BW model) and Al–Cu (PAN model) are given in Figs. 2 and 3, respectively. Tabor's relation is superimposed to these figures, where

Table 1
Extracted properties through Tabor's relation (Eq. (1)).

	$\sigma_\circ$ (MPa)	n	E^a (GPa)
Al–Cu (PAN model)	590	0.2	70
Pure Cu (Modified-BW model)	670	0.65	110

[a] Young's modulus assumed for an equivalent polycrystalline aggregate.

the values of $\sigma_\circ$ and n (Table 1) were found a priori by fitting the data of the single-crystal hardness evolutions to the logarithmic reformulation of Eq. (1)

$$\ln \bar{p} = \ln(2.8\sigma_\circ) + n \ln\left(0.4\frac{a}{D}\right) \tag{12}$$

It is noted that while unique values of $\sigma_\circ$ and n can indeed be used in conjunction with Tabor's relation to describe the entire normalized hardness evolutions for pure copper, this is not the case for Al–Cu where the constancy in n is only found in the range of $0.07 < a/D < 0.16$. Hence, in the latter simulations, a consistent shift to smaller hardnesses is found in the lower region of $aE/D\sigma_\circ$ as compared with predictions from Tabor's relation (Fig. 3).

Following Ref. [1], the above results are taken to indicate that Tabor's relation can be accurately used to describe single-crystal indentation experiments and that a decrease of hardness from the predicted values at low a/D marks attainment of the elasto-plastic indentation regime. The present analysis thus favors the view that Tabor's relation represents an upper bound for the hardness evolutions [31]. Moreover, this interpretation illustrates the pivotal role that the critical shear stress for dislocation gliding $\tau_\circ$ plays in inducing elasto-plasticity, as this regime only becomes evident under marked values of $\tau_\circ$ as in the PAN model.

Interestingly, note that the J_2-flow theory finite element simulations performed for the extracted values of $\sigma_\circ$ and n from the modified-BW and PAN models (Table 1), accurately trace the crystal plasticity simulations throughout the entire range of parameter $aE/D\sigma_\circ$ (see Figs. 2 and 3). Although this result is not surprising because Tabor's relation is supported under J_2-plasticity theory analyses (e.g., [31]), it is interesting to find that such simulations reproduce the single-crystal hardness evolution for the PAN model even though the inferred n and $\sigma_\circ$ were obtained by neglecting the lower elasto-plastic penetration range of $a/D < 0.07$. It thus necessarily follows that since elasto-plasticity is a natural outcome of J_2-flow simulations at small penetrations, where the full set of Eqs. (2)–(4) with non-vanishing σ_{ys} is enforced, the mechanical properties inferred within the fully-plastic regime are valid for the entire hardness evolutions as they are indeed consistent with the actual σ_{ys} in the material.

It is worth noting that the task of extracting mechanical properties from Tabor's relation may be difficult to accomplish in crystals with marked values of $\tau_\circ$, where the range of validity of this relation is reduced as the aforementioned elasto-plastic regime rules the indentation behavior within a wide range of values of a/D. Under such contact conditions, a general formulation for the hardness evolution in terms of the mechanical properties and a/D has been recently found by the present authors covering both elasto-plastic and fully-plastic spherical indentations (see Flow Chart 1 in [31]). The use of this relation in mechanical property extractions is therefore recommended over Tabor's formula, which can only be enforced in crystals exhibiting predominantly fully-plastic indentation responses throughout a sufficiently large range of a/D.

Finally, attention is directed to the hardness decay found for the PAN model at large penetrations (see $(E/\sigma_\circ)a/D > 14$ in Fig. 3). This decay has been found to occur in weak strain hardening solids obeying the J_2-flow plasticity theory (i.e., the so-called perfect-plasticity dominated regime in our recent work [31]). In this sense, it is worth noting that the inferred value of $n \approx 0.2$ for the PAN model is not small enough as to favor a decay in hardness for the equivalent J_2-flow theory analysis superimposed in Fig. 3. This indicates that while the inferred mechanical properties can be used in reproducing the single-crystal behavior at small penetrations, the same is not true at greater penetrations where strain hardening may become gradually milder as illustrated in Fig. 1 for the PAN model. This is an interesting result illustrating the potential of spherical indentation in probing the cross-hardening deformation stage-II at small values of a/D as well as the strong stage-III hardening saturation behavior of alloyed fcc crystals at greater values of a/D.

4. The possible violation of self-similarity in fully-plastic indentations

It is noteworthy that the fundamental mechanistic origin to the onset of elasto-plasticity concerns attainment of significant elastic strains in the indentation behavior. This aspect can be readily extended to single-crystal indentations by invoking a parallel between the roles of marked values of $\tau_\circ$ and σ_{ys} upon the contact response.

As discussed next, an interesting feature that emerges from the present simulations is that the onset of full-plasticity does not ensure attainment of self-similar indentation responses, where both the relative plastic zone size with respect to contact radius a as well as parameter c^2 would have been taken to remain constant as the experiment progresses. This issue can be readily examined from Fig. 4, showing the evolution of parameter c^2 for the modified-BW and PAN models. The present results show that while c^2 remains constant in the simulations under the modified-BW model, in agreement with the assumption of fully-plastic self-similar indentations, this constancy is not attained for the PAN formulation even within the intermediate penetration range ($0.07 < a/D < 0.16$) where Tabor's relation becomes valid. It therefore follows

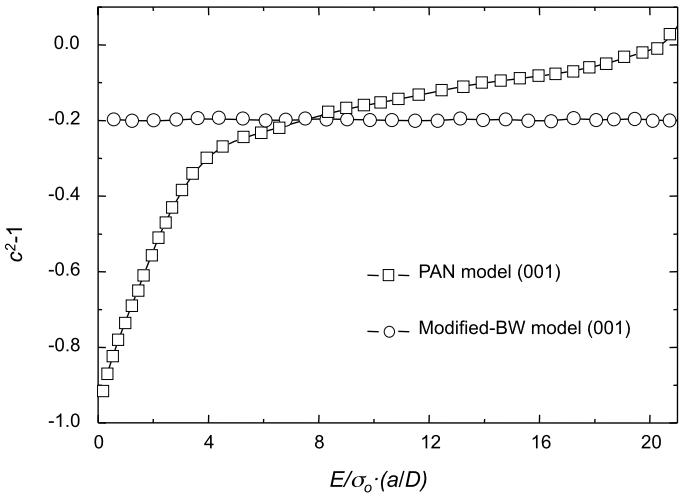

Fig. 4. Evolution of pile-up/sinking-in parameter c^2 for the PAN and modified-BW models. Notice that while self-similarity rules the response under the modified-BW model, the constancy in c^2 is violated for the PAN model even in the range of $E/\sigma_\circ \cdot (a/D) > 7$ setting the fully-plastic indentation regime according to Tabor's relation (see Fig. 3).

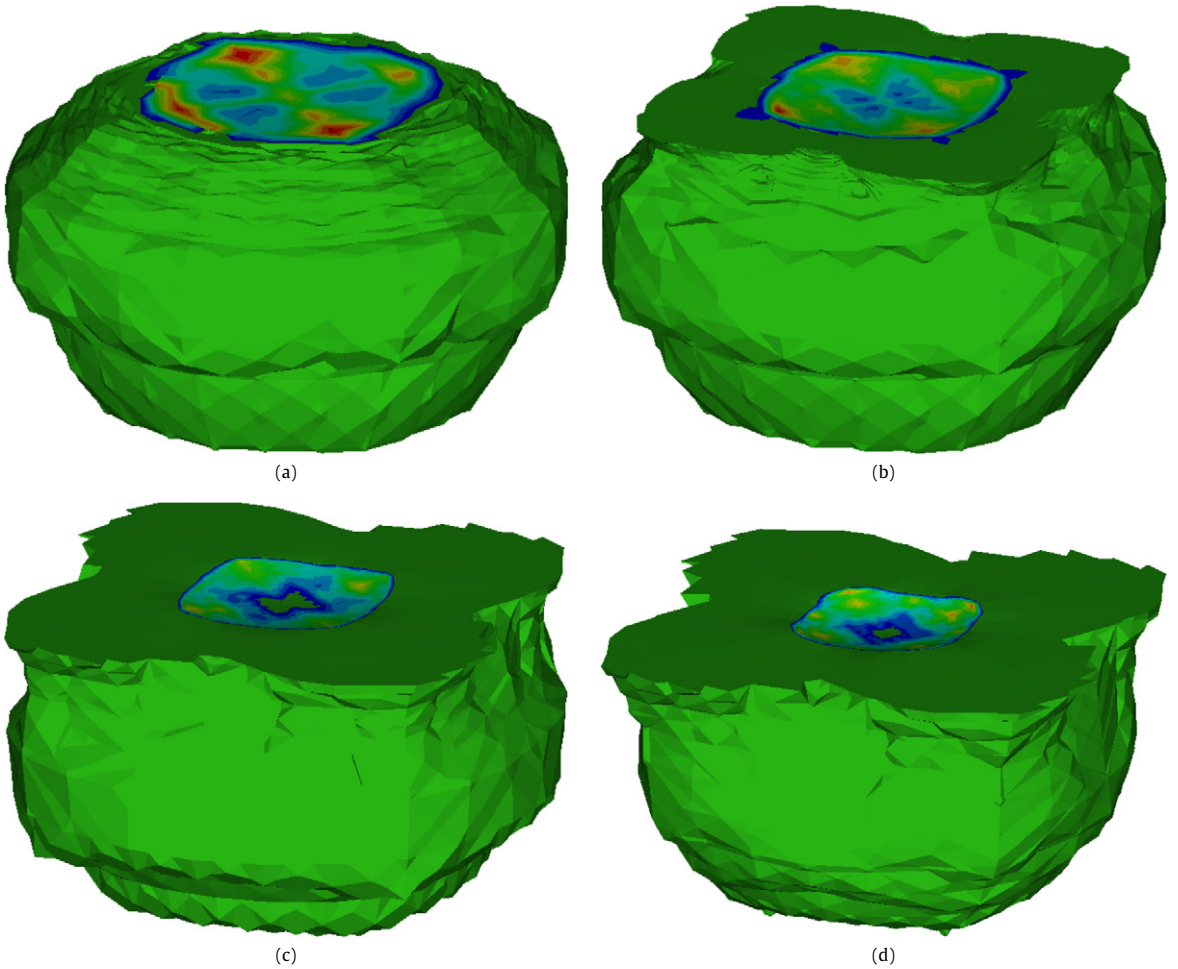

Fig. 5. Evolution of the plastic zone shape for the PAN model as given by the three-dimensional isocontour of total accumulated shear strain $\gamma = 5 \times 10^{-4}$ for (001)-indentation: (a) $a/D = 0.035$; (b) $a/D = 0.060$; (c) $a/D = 0.090$; (d) $a/D = 0.140$. Notice that the spreading of plasticity at the surface is gradually enhanced even above the value of $a/D > 0.07$ $(E/\sigma_\circ \cdot (a/D) > 7)$ marking the onset of the fully-plastic regime in Fig. 3.

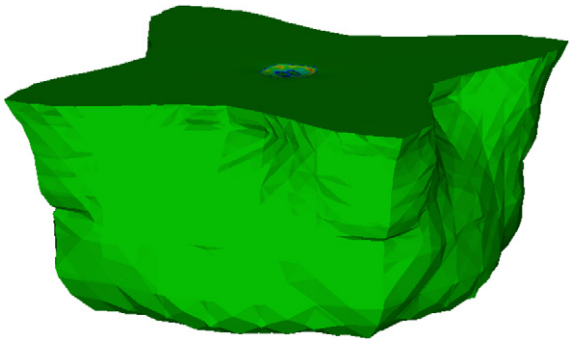

Fig. 6. Plastic zone shape for the modified-BW model as given by the three-dimensional isocontour of total accumulated shear strain $\gamma = 5 \times 10^{-4}$ for (001)-indentation at $a/D = 0.08$. The plastic zone is found to scale in a self-similar fashion with increasing a regardless of the imposed value of a/D.

that while Tabor's relation is a general fully-plastic upper hardness bound, its validity does not truly require fulfillment of self-similarity [31].

The above conceptions are further sustained upon examination of the plastic zone shapes in Figs. 5 and 6. In this sense, it is found that while the plastic zone size scales in a self-similar manner in the simulations with the modified-BW model, this feature is violated for the PAN model where the outwards spreading of the plastic zone is greater than the increase in contact radius a. It is again interesting to notice that the lack of the self-similar scaling in the plastic zone extends into the regime where Tabor's equation becomes an accurate representation to the hardness evolutions.

4.1. Concluding remarks

We have illustrated the use of Tabor's hardness relation, which was originally postulated for polycrystalline aggregates, into the analysis of single-crystal spherical indentations. In pure fcc crystals with vanishing critical shear strength for dislocation gliding $\tau_\circ$, hardness $\bar{p}$ thus increases as the ratio between contact radius and indenter diameter, a/D, is raised following Eq. (1). Tabor's formula thus preserves its character as upper fully-plastic bound found in prior investigations for polycrystalline aggregates [31]. In contrast to the results from the present simulations with the modified-BW model, elasto-plastic single-crystal spherical indentation behaviors are illustrated in the simulations performed for alloyed crystals with marked $\tau_\circ$ through the PAN model. In these crystals, hardness lies below predictions from Tabor's formula for small values of a/D while, with increasing penetration, this formula becomes applicable. In view of these results, a few remarks are given in the text concerning the extraction of flow properties $\sigma_\circ$ and n from Tabor's relation ruling single-crystal cross-hardening deformation stage-II, as well as the assessment of strain hardening saturation (deformation stage-III) at large values of a/D.

This investigation also illustrates on the strictness of the assumption of self-similarity to single-crystal indentations. It is found that while Tabor's relation is an accurate fully-plastic bound as indicated above, the onset of fully-plastic indentation responses does not necessarily underly attainment of self-similarity. In this sense, the simulations with the modified-BW model show that while the plastic zone size and the material pile-up/sinking-in response respectively scale in proportion with contact radius a and penetration depth h, these features are not preserved in the fully-plastic indentation regime of alloyed crystals with a marked $\tau_\circ$ deforming through the PAN model. The self-similar scaling of the contact response with penetration in the simulations with the PAN model is therefore violated even within the fully-plastic indentation regime where Tabor's formula rules the indentation behavior.

Acknowledgement

The authors acknowledge financial support by the Spanish Ministry of Education and Science through project MAT2008-01647/MAT.

References

[1] K.L. Johnson, Contact Mechanics, Cambridge University Press, United Kingdom, 1985.
[2] R. Hill, E.H. Lee, S.J. Tupper, The theory of wedge indentation of ductile materials, Proc. R. Soc. London A 188 (1947) 273–289.
[3] A.J. Ishlinsky, An axi-symmetrical problem in plasticity and the Brinell test, Appl. Math. Mech. 8 (1944) 201–224.
[4] D. Tabor, Hardness of Metals, Clarendon Press, Oxford, United Kingdom, 1951.
[5] M. Mata, M. Anglada, J. Alcalá, A hardness equation for sharp indentation of elastic-power-law strain-hardening materials, Philos. Mag. A 82 (2002) 1831–1839.
[6] M. Mata, O. Casals, J. Alcalá, The plastic zone size in indentation experiments: The analogy with the expansion of a spherical cavity, Int. J. Solids Struct. 43 (2006) 5994–6013.
[7] X.L. Gao, X.N Jing, G. Subhash, Two new expanding cavity models for indentation deformations of elastic strain-hardening materials, Int. J. Solids Struct. 43 (2006) 2193–2208.
[8] D. Durban, R. Masri, Conical indentation of strain hardening solids, Eur. J. Mech. A – Solids 27 (2008) 210–221.

[9] P. Jiang, T. Zhang, Y. Feng, R. Yang, N. Liang, Determination of plastic properties by instrumented spherical indentation: Expanding cavity model and similarity solution approach, J. Mater. Res. 24 (2009) 1045–1053.
[10] R. Hill, B. Störakers, A.B. Zdunek, A theoretical study of the Brinell hardness test, Proc. R. Soc. London A 423 (1989) 301–330.
[11] X. Hernot, O. Bartier, Y. Bekouche, Y.R. El Abdi, G. Mauvoisin, Influence of penetration depth and mechanical properties on contact radius determination for spherical indentation, Int. J. Solids Struct. 43 (2006) 4136–4153.
[12] K.D. Bouzakis, N. Michailidis, An accurate and fast approach for determining materials stress–strain curves by nanoindentation and its FEM-based simulation, Mater. Charact. 56 (2006) 147–157.
[13] H.Z. Lan, T.A. Venkatesh, On the sensitivity characteristics in the determination of the elastic and plastic properties of materials through multiple indentation, J. Mater. Res. 22 (2007) 1043–1063.
[14] S. Ghosh, T.K. Pal, S. Mukherjee, G. Das, S. Ghosh, Comparative study of heat-affected zone with weld and base material after post-weld heat treatment of HSLA steel using ball indentation technique, J. Mater. Sci. 43 (2008) 5474–5482.
[15] T.H. Zhang, P. Jiang, Y.H. Feng, Numerical verification for instrumented spherical indentation techniques in determining the plastic properties of materials, J. Mater. Res. 24 (2009) 3653–3663.
[16] M. Beghini, L. Bertini, V. Fontanari, B.D. Monelli, Numerical analysis of plastic deformation evolution into metallic materials during spherical indentation process, J. Mater. Res. 24 (2009) 1270–1278.
[17] A. Yonezu, Y. Kuwahara, K. Yoneda, H. Hirakata, K. Minoshima, Estimation of the anisotropic plastic property using single spherical indentation – An FEM study, Comput. Mater. Sci. 47 (2009) 611–619.
[18] S.K. Kang, J.Y. Kim, I. Kang, D. Kwon, Effective indenter radius and frame compliance in instrumented indentation testing using a spherical indenter, J. Mater. Res. 24 (2009) 2965–2973.
[19] J.H. Lee, T. Kim, H. Lee, A study on robust indentation techniques to evaluate elastic–plastic properties of metals, Int. J. Solids Struct. 47 (2010) 647–664.
[20] Y. Wang, D. Raabe, C. Kluber, F. Roters, Orientation dependence of nanoindentation pile-up patterns and of nanoindentation microtextures in copper single crystals, Acta Mater. 52 (2004) 2229–2238.
[21] C. Zambaldi, F. Roters, D. Raabe, U. Glatzelb, Modeling and experiments on the indentation deformation and recrystallization of a single-crystal nickel-base superalloy, Mater. Sci. Eng. A 454–455 (2007) 433–440.
[22] O. Casals, J. Ocenasek, J. Alcalá, Crystal plasticity finite element simulations of pyramidal indentation in copper single crystals, Acta Mater. 55 (2007) 55–68.
[23] Y. Liu, S. Varghese, J. Ma, M. Yoshino, H. Lu, R. Komanduri, Orientation effects in nanoindentation of single crystal copper, Int. J. Plasticity 24 (2008) 1990–2015.
[24] J. Alcalá, O. Casals, J. Ocenasek, Micromechanics of pyramidal indentation in fcc metals: single crystal plasticity analysis, J. Mech. Phys. Solids 56 (2008) 3277–3303.
[25] J. Alcala, D. Esque-de los Ojos, S.A. Rodriguez, The role of crystalline anisotropy in mechanical property extractions through Berkovich indentation, J. Mater. Res. 24 (2009) 1235–1244.
[26] Z.L. Liu, X.M. Liu, Z. Zhuang, X.C. You, A multi-scale computational model of crystal plasticity at submicron-to-nanometer scales, Int. J. Plasticity 25 (2009) 1436–1455.
[27] R.J. Asaro, Micromechanics of crystals and polycrystals, Adv. Appl. Mech. 23 (1983) 1–115.
[28] J. Alcalá, O. Casals, J. Ocenasek, Corrigendum to “Micromechanics of pyramidal indentation in fcc metals: Single crystal plasticity finite element analysis” [J. Mech. Phys. Solids 56 (2008) 3277–3303], J. Mech. Phys. Solids 58 (2010) 751.
[29] D. Peirce, R.J. Asaro, A. Needleman, An analysis of nonuniform and localized deformation in ductile single-crystals, Acta Metall. 30 (1982) 1087–1119.
[30] D. Peirce, R.J. Asaro, A. Needleman, Material rate dependence and localized deformation in crystalline solids, Acta Metall. 31 (1983) 1951–1976.
[31] J. Alcalá, D. Esque-de los Ojos, Reassessing spherical indentation: contact regimes and mechanical property extractions, Int. J. Solids Struct. 47 (2010) 2714–2732.